Supporting Information

Supporting Information Corrected June 27, 2014

Ewers et al. 10.1073/pnas.1300772110

SI Results

Tyrosinate Fluorescence in WT Glt_{Ph}. Exciting WT Glt_{Ph} at 295 nm, which is commonly done to elicit tryptophan emission (1), results in fluorescence with a maximum at ∼320 nm, which is similar to the values observed for L130W Glt_{Ph} (Fig. 1*D*). The tyrosine emission spectra normally peak at wavelengths close to 300 nm; however, ionization of tyrosine residues causes a red shift in excitation as well as emission maxima (2), which explains the observed WT Glt_{Ph} fluorescence properties in the absence of any tryptophan residues. The small increase that is only found at lower wavelengths after Na^+ addition to WT Glt_{Ph} resembles the effect of Na^+ on L130W Glt_{Ph} fluorescence and might have the same origin. After 289 nm excitation, the WT Glt_{Ph} emission peaks at 306 nm (Fig. 1*E*), which indicates that the emission of protonated tyrosine residues instead of tyrosinates is dominating at this excitation wavelength.

Slow Transitions Associated with Na^+ Binding. The observed [Na^+] dependence of the time course of the fluorescence signals on aspartate addition (Fig. 2) indicates slow processes that precede fast amino acid binding to Glt_{Ph}. To study these slow processes in greater detail, we performed the simultaneous rapid addition of varying [Na^+] and a fixed [L-aspartate] of 500 μM, which resulted in a clear increase in the overall rate of fluorescence change with increasing [Na^+] (Fig. S1). This observation shows the contribution of one or more Na^+ binding steps to the observed transitions. The observed left shift of the curves on the time axis with increasing [Na^+] indicates an increase in the value of the rate of one or more processes as opposed to an increase in the amplitude of faster processes. Thus, at least one of the processes involved occurs after Na^+ binding. The complexity of the kinetics, in addition to the uncertainties inherent in fitting the sums of many exponential functions to the kinetic data, precludes a detailed quantitative analysis here.

The equilibrium Na^+ binding properties are only marginally affected by the L130W mutation (Fig. 2*D*). Nevertheless, L130W still could have changed the kinetics of Na^+ binding. To assess the general validity of the observed slow transients of Na^+ binding to L130W Glt_{Ph}, we measured the stopped-flow kinetics of Na^+ (250 mM) binding to WT Glt_{Ph} by monitoring tyrosine fluorescence after excitation at 289 nm. We observed a similar time course (Fig. S2) as compared to the time course after the simultaneous addition of L-aspartate and Na^+ to L130W Glt_{Ph}. The comparison of $t_{1/2}$ values as a measure of overall rate (0.42 s; after the addition of 250 mM Na^+ and 500 μM L-aspartate to L130W Glt_{ph}: 0.1 s) (Fig. S2) shows that the slow kinetics of Na^+ binding to L130W Glt_{Ph} are not caused by the introduced tryptophan and that L130W is a reasonable reporter mutation to monitor the kinetics of substrate binding to Glt_{Ph}.

L-Cysteine Sulfinic Acid Is Transported with a Lower Affinity than L-Aspartate. L-cysteine sulfinic acid (L-CS) exhibits an ≈10-fold lower binding affinity to Glt_{Ph} than L-aspartate, which was shown using the variation in fluorescence of W130 (2). To examine whether this difference is maintained during transport, we measured ^{3}H-L-aspartate uptake by Glt_{Ph} into proteoliposomes. Fig. S3*A* shows that, in presence of 10 μM cold L-aspartate, the rate of ^{3}H-L-aspartate transport was reduced to the level of uptake into liposomes without Glt_{Ph}. In contrast, 10 μM L-CS did not completely abolish ^{3}H-L-aspartate transport but resulted in an ≈90% inhibition (Fig. S3*B*). Therefore, L-CS displays a lower affinity to Glt_{Ph} than L-aspartate also under transport conditions.

To assess the relative transport activities of L-aspartate and L-CS, we compared the ability of saturating concentrations of the amino acids inside the proteoliposomes to stimulate ^{3}H-L-aspartate uptake by counterflow. A similar assay was previously used to compare transport activities of potential substrates of mammalian glutamate transporters, with the difference that the ability of external amino acids to stimulate efflux of D-aspartate from synaptosomes was tested (3). Fig. S3*C* shows that L-aspartate and L-CS inside the proteoliposomes increase the amount of ^{3}H-L-aspartate that is transported after 5 min to the same degree, whereas D,L-threo-β-benzyloxyaspartate (TBOA), which is thought to be a non-transportable inhibitor, does not cause an increase. We conclude that L-CS is a transported substrate of Glt_{Ph} and that L-aspartate and L-CS have comparable transport activities.

Simulation of Time-Dependent Fluorescence Changes on Amino Acid Addition. To test the accuracy of the derived model parameters of amino acid binding (Table 1), we simulated time courses on substrate addition through the integration of the corresponding differential equations. The model predicts an initial lag phase at low concentrations of amino acids that is most pronounced with L-CS. To ensure comparability, the simulated traces were treated the same way as the experimental data by extrapolating to time 0 after fitting with an exponential function (*SI Materials and Methods*).

Fig. S4 shows the simulated traces after such treatment along with the normalized experimental traces after L-aspartate, D-aspartate, and L-CS addition, which resulted from a range of starting parameters. The curve shapes of the simulated and experimental traces for all substrates agree over the entire substrate concentration range. To evaluate the sensitivity of the kinetics to changes in the model parameters in relation to experimental scatter, we produced additional simulations with single parameters outside the 95% confidence intervals, which are presented in Table 1. We focused on the parameters that were determined to be significantly different between the substrates, such as the dissociation rate constants of the first step (k_{off}) as well as the forward rate constants of the conformational change (k_1). For such simulations, values equidistant to the respective confidence interval boundaries were selected. The resulting traces, after exponential fitting and normalization, in some cases show remarkable changes in curve shape (e.g., when increasing k_1 of L-CS binding at high concentrations) (Fig. S4*C*). Other deviations are more subtle but are found over the entire range from lower to higher micromolar concentrations, such as the deviations arising from decreasing the k_1 of D-aspartate binding (Fig. S4*B*). When decreasing the k_1 of L-aspartate binding (Fig. S4*A*), the traces originating from a small range of concentrations (5–10 μM L-aspartate) clearly indicate inadequacy of the model that contains the altered parameter. Altogether, the simulations show the sufficient sensitivity of our experimental system to discriminate between the tested model parameters of the different substrates.

Derivation of the Kinetic Equations. For the reaction scheme,

$$P + L \underset{k_{off}}{\overset{k_{on}}{\rightleftharpoons}} PL \underset{k_2}{\overset{k_1}{\rightleftharpoons}} P^*L,$$

assuming [*L*] >> [P], [PL], and [P*L], the time-dependent relaxation of [P], [PL], and [P*L] to the new equilibrium after ligand concentration changes can be described by the transition matrix (TM):

$$TM = \begin{bmatrix} -[L]k_{on} & k_{off} & 0 \\ [L]k_{on} & -k_1 - k_{off} & k_2 \\ 0 & k_1 & -k_2 \end{bmatrix}.$$

Solving the eigenvalue problem of TM yields a set of two nonzero eigenvalues and corresponding eigenvectors, with

$$k_{obs1} = -\lambda_1 \text{ and}$$

$$k_{obs2} = -\lambda_2.$$

Finding the eigenvalues of TM is equivalent to transforming TM to a singular matrix with a determinant zero by subtracting a scalar matrix $\lambda \cdot I$ (I being an identity matrix of the same size as TM):

$$\det(TM - \lambda \cdot I) = 0$$

or

$$\det(TM + k_{obs}) = 0:$$

$$\det \begin{bmatrix} k_{obs} - [L]k_{on} & k_{off} & 0 \\ [L]k_{on} & k_{obs} - k_1 - k_{off} & k_2 \\ 0 & k_1 & k_{obs} - k_2 \end{bmatrix} = 0.$$

Calculating the determinant leads to

$$k_{obs}^3 - k_2 k_{obs}^2 - k_{obs}^2 k_{off} - k_1 k_{obs}^2 - k_2 k_{obs} k_{off} - [L]k_{obs}^2 k_{on} + [L]k_1 k_{obs} k_{on} + [L]k_2 k_{obs} k_{on} = 0$$

and

$$k_{obs}\left[k_{obs}^2 - k_{obs}\left(k_2 + k_{off} + k_1 + [L]k_{on}\right) + \left(k_2 k_{off} + [L]k_1 k_{on} + [L]k_2 k_{on}\right)\right] = 0.$$

Nonzero solutions for k_{obs} are obtained by setting the second factor to zero:

$$k_{obs}^2 - k_{obs}\left(k_2 + k_{off} + k_1 + [L]k_{on}\right) + \left(k_2 k_{off} + [L]k_1 k_{on} + [L]k_2 k_{on}\right) = 0.$$

The two solutions are

$$k_{obs_1} = \frac{1}{2}\left(k_{on}[L] + k_{off} + k_1 + k_2\right) + \frac{1}{2}\sqrt{\left(k_{on}[L] + k_{off} + k_1 + k_2\right)^2 - 4\left(k_{on}(k_1 + k_2)[L] + k_{off}k_2\right)}$$
$$= \frac{1}{2}\left[\left(k_{on}[L] + k_{off} + k_1 + k_2\right) + \sqrt{\left(k_{on}[L] + k_{off} - k_1 - k_2\right)^2 + 4k_1 k_{off}}\right]$$

and

$$k_{obs_2} = \frac{1}{2}\left(k_{on}[L] + k_{off} + k_1 + k_2\right) - \frac{1}{2}\sqrt{\left(k_{on}[L] + k_{off} + k_1 + k_2\right)^2 - 4\left(k_{on}(k_1 + k_2)[L] + k_{off}k_2\right)}$$
$$= \frac{1}{2}\left[\left(k_{on}[L] + k_{off} + k_1 + k_2\right) - \sqrt{\left(k_{on}[L] + k_{off} - k_1 - k_2\right)^2 + 4k_1 k_{off}}\right] (4).$$

SI Materials and Methods

Mutagenesis, Expression, and Purification of Glt_{Ph}. L130W was inserted into pBAD24-Glt_{Ph}, which encodes the WT Glt_{Ph} with a C-terminal 8× histidine tag (provided by Eric Gouaux, Oregon Health and Science University, Portland, OR) using the QuikChange Kit (Stratagene). *Escherichia coli* Top10 or BL21-AI cells (Invitrogen) harboring one of the resulting plasmids and in the case of Top10, pLysN to facilitate later bacterial lysis (5) were grown to OD_{500} = 0.5–0.7. After induction with 1% L-arabinose, the cells were incubated for 4 h. The following steps were performed at 4 °C. The cells were harvested by centrifugation. Lysis was performed by sonication followed by centrifugation at 15,000 × *g* to remove cellular debris. The supernatant was centrifuged at 100,000 × *g*. The resulting crude membranes were resuspended in 20 mM Tris (pH 7.4), 200 mM NaCl, and 250 mM sucrose and solubilized by the dropwise addition of 40 mM n-dodecyl-β-D-maltopyranoside (DDM) (GLYCON Biochemicals) while stirring. After 1 h, DDM was diluted to 10 mM, and imidazole was supplemented to 30 mM. The insoluble material was pelleted by centrifugation at 65,000 × *g* for 30 min; 1 mL nickel-nitrilotriacetic acid agarose (Qiagen) was added per 1 mg expected Glt_{Ph} yield, and the mixture was incubated overnight at 4 °C. Subsequently, the affinity resin with bound proteins was washed with six volume equivalents of 20 mM Tris (pH 7.4), 200 mM NaCl, 41.25 mM imidazole, and 1 mM DDM. The elution was performed with 20 mM Tris (pH 7.4), 200 mM NaCl, 500 mM imidazole, and 1 mM DDM. No preparative size exclusion chromatography was performed. The purity and size distribution of Glt_{Ph} was assessed by SDS/PAGE and analytical size exclusion chromatography on a Superdex 200 10/300GL column (GE Healthcare) equilibrated in a buffer containing 100 mM Tris (pH 8), 200 mM NaCl, 5 mM EDTA, and 1 mM DDM. The [protein] was estimated from the absorbance of the solution at 280 nm using a molar extinction coefficient of 57,400 M^{-1} cm^{-1} for WT Glt_{Ph} (6). To obtain the molar extinction coefficient for L130W Glt_{Ph} (62,400 M^{-1} cm^{-1}), we added to this value the contribution of a single additional tryptophan (7). The purified protein was flash frozen and stored at −80 °C until use.

To remove Na^+ and potentially bound amino acids, NaCl was replaced by choline chloride in four successive purification steps using disposable desalting columns (GE Healthcare) followed by two additional steps with background buffer if necessary. All buffers contained 20 mM Tris (pH 7.4), 1 mM DDM, and choline chloride or NaCl as reported in the figures. If necessary, the proteins were concentrated using ultrafiltration cartridges (100-kDa exclusion limit; Millipore) after thawing.

Cysteine Cross-Linking. Cu(II)(1,10-phenanthroline)$_3$-mediated cross-linking was performed as previously described (8). For the cross-linking of L130W K55C C321S A364C Glt_{Ph}, samples were incubated for 1 h with 10 mM DTT to reduce cysteines. Samples of both cysteine mutants were subjected to three successive rounds of buffer exchange to 20 mM Tris (pH 7.4), 1 mM DDM, and 200 mM choline chloride using disposable desalting columns. The oxidative cross-linking was performed for 30 min or 1 h with 0.1 or 1 mM Cu^{2+} and 1,10-phenanthroline freshly mixed at a 1:2 molar ratio. The reactions were quenched with 10 mM *N*-ethylmaleimide. Before fluorescence measurements, L130W K55C C321S A364C Glt_{Ph} was subjected to two rounds of buffer exchange into 20 mM Tris (pH 7.4), 1 mM DDM, and 200 mM choline chloride. In the case of L130W V261C C321S A391C Glt_{Ph}, two successive rounds of buffer exchange into 20 mM Tris (pH 7.4), 1 mM DDM, and 200 mM NaCl were performed before nonreducing SDS/PAGE and fluorescence measurements. To compare the electrophoretic mobility of single and double cysteine mutants unbiased by the oxidative treatments, electrophoresis was performed directly after affinity chromatography. To quantify the relative amounts of protein in Coomassie Brilliant Blue-stained gels, the OD was compared with the ODs of a calibrated transmission step wedge (T2115; Stouffer).

Fluorescence Measurements and Data Analysis. The fluorescence spectra of the WT and mutant Glt_{Ph} were determined in a Quantamaster 4 spectrofluorometer (Photon Technology Inc.), with the excitation and emission slits set to a band pass of 4 and 5 nm, respectively. The sample solution was stirred in a 1-cm cuvette thermostated to 22 °C. The measured photomultiplier photon counts were corrected for the instrumental wavelength dependency and excitation intensity. To obtain the Glt_{Ph} fluorescence intensities, the background signal was subtracted from the signal of the same cuvette containing 0.1–1 μM Glt_{Ph}. The fluorescence responses to Na^+ were registered after adding aliquots of concentrated stock solutions. The fluorescence intensity data were corrected for the error resulting from a decreased concentration of the fluorophore on the addition of any solution volume.

To monitor changes in Glt_{Ph} fluorescence on the rapid addition of Na^+ or amino acids, a stopped-flow apparatus was used (HITECH SF-61SX2/s; TgK Scientific). Excitation was generated through a monochromator set at 297 nm unless otherwise specified. Emission wavelengths were selected using a long-pass glass filter (cut-on wavelength: 320 nm; WG320; SCHOTT) or a long-pass interference filter (cut-on wavelength: 306 nm; BrightLine HC 300/LP; Semrock) that resulted in a higher signal-to-noise ratio. The dead time of the system (i.e., the time between the initiation of the reaction and the first usable data point), was determined by monitoring the bleaching of *N*-acetyltryptophanamide fluorescence by *N*-bromosuccinimide at different concentrations (9). Single exponential functions were fitted to the traces, and the dead time was calculated according to $deadtime = \frac{-\ln(a_{obs})}{k_{obs}}$, where a_{obs} represents the relative observed amplitude. For the standard configuration of the instrument with an observation cell containing 22 μL, this procedure resulted in a value of 2.3 ± 0.1 ms ($n = 4$). When measuring the binding of L-aspartate to Na^+-bound Glt_{Ph} at higher temperatures, a cell with a volume of 5 μL and a determined dead time of 0.9 ± 0.1 ms ($n = 5$) was used. Unless otherwise specified, the mixing system and observation cell were thermostated to 6 °C. The [Glt_{Ph}] ranged from 0.05 to 4 μM, and the [amino acid] was maintained at a concentration of at least fivefold molar excess over the [Glt_{Ph}] to fulfill pseudo-first order conditions (10). Fluorescence was acquired on a linear time base for closely spaced processes and a logarithmic time base for largely separated processes. Before analysis, between 2 and 15 traces were averaged. Data analysis was performed using Origin (OriginLab). After fitting exponential functions to the data, a homogeneous distribution of the residuals around zero was collected as a criterion to select the appropriate fit. Presumably, because of variations in the buffers, trace-to-trace reproducibility of the signal level was poor in many of our measurements. All amplitudes of fluorescence changes were inferred from the fit result extrapolated to time 0. During the fits of Eq. **1** to [amino acid] dependencies of $k_{obs,fast}$, all parameters were constrained to positive values. The value of k_2 was fixed to 10 s^{-1}. Asymptotic confidence intervals were computed from the fit residuals by the fitting software.

Factor Xa-Mediated Proteolysis. To generate the factor Xa cleavable mutant, 111AGIH114 was replaced by IDGR on the background of L130W Glt_{Ph}. The cleavage of AGIH111-114IDGR L130W Glt_{Ph} was performed as previously described (11). Briefly, the protein sample buffer was exchanged to 20 mM Tris/Hepes (pH 8), 100 mM NaCl, 5 mM $CaCl_2$, and 7 mM DDM using disposable desalting columns. Cleavage was performed by the addition of Factor Xa (activated bovine Factor X; Sigma) at a ratio of 40 μg to 1 mg protein for 48 h at 37 °C. Thrombin was added at 30 U/mg protein after 8 h. Later, this step was omitted, because the His-tag does not modify the fluorescence properties. The reaction was stopped by the addition of 1 mM 4-(2-aminoethyl)-benzenesulfonyl fluoride and 10 mM EDTA.

Reconstitution of Glt_{Ph} into Liposomes and Transport Assay. Glt_{Ph} was reconstituted into liposomes according to information in ref. 12; control liposomes without Glt_{Ph} were prepared in parallel under identical conditions. Proteoliposomes and control liposomes (20 mg lipid/mL) were flash frozen in liquid nitrogen and stored at −80 °C. Proteoliposomes and control liposomes were loaded with 100 mM KCl and 20 mM Hepes (pH 7.5) by at least three freeze/thaw cycles and extrusion (10 times through two 400-nm pore size polycarbonate filters; Avestin). The uptake reaction was initiated by the addition of 1 μL proteoliposomes/control liposomes (100–125 mg lipid/mL) to 199 μL external buffer (100 mM NaCl, 20 mM Hepes, pH 7.5, 1 μM valinomycin, 100 nM ^{3}H-L-aspartate, additives as indicated). External buffers were preequilibrated at 30 °C, and after the addition of liposomes, the mixture was briefly mixed. At each time point, the reactions were quenched by addition of 1.8 mL ice-cold 150 mM KCl followed by immediate suction filtration over nitrocellulose filters (0.22-μm pore size; GSWP; Millipore). The filters were washed three times with 1.8 mL ice-cold quench buffer. Radioactivity trapped on the filters was measured by addition of 10 mL Filter-Count (PerkinElmer), and subsequent counting in a TRI-CARB 2000CA scintillation counter (PerkinElmer). The signal-to-background ratio (dpm proteoliposomes/dpm control liposomes) was 400–500 at a reaction time of 6 min. Initial rates were calculated from the linear portion of the uptake time courses (first 60 s).

For counterflow experiments, proteoliposomes were loaded with 100 mM NaCl, 20 mM Hepes (pH 7.5) alone or with buffer, and 50 μM L-aspartate, L-CS, or DL-TBOA, respectively. The proteoliposomes were concentrated and washed by centrifugation (270,000 × *g*, 25 min, 4 °C). The pellets were resuspended in 100 mM NaCl and 20 mM Hepes, pH 7.5 (60 mg lipid/mL). The reaction was initiated by the addition of 194–198 μL prewarmed external buffer (100 mM NaCl, 20 mM Hepes, pH 7.5, 100 nM ^{3}H-L-aspartate) to 2–6 μL proteoliposomes. The mixture was briefly vortexed, and at each time point, the reactions were quenched by the addition of 1.8 mL ice-cold quench buffer (100 mM NaCl, 20 mM Hepes, pH 7.5) followed by immediate filtration over nitrocellulose filters. The filters were washed, and the radioactivity was measured as described above. Data analysis was done with GraphPad Prism (GraphPad Software).

Simulation of Time-Dependent Fluorescence Changes. Amino acid binding to Glt_{Ph} was simulated using COPASI (13). Differential equations corresponding to Scheme **1** were solved by the implemented Livermore Solver for Ordinary Differential Equations (14) using the values presented in Table 1. To ensure the comparability of the simulated and experimental curves, the simulations were started from the end of the dead time of the stopped-flow apparatus (2.3 ms), and the resulting curves were fitted with an exponential function (one exponential term) extrapolating to time 0. The results were normalized to values between zero and one, P was assigned a relative fluorescence change of zero, and P* was assigned a change of one. Through this procedure, which is analogous to the treatment of the experimental data, deviations from a single exponential behavior in the simulated curves (i.e., the initial lag phase that was observed at low amino acid concentrations) that are not contained in the experimental curves are absent in the simulated data as well. Therefore, the progress of curves from time 0 to the end of the dead time is determined by the extrapolation of the fitted exponential only, which reproduces the information loss concerning the signal amplitude in the dead time of the stopped-flow apparatus.

1. Lakowicz J (2006) *Principles of Fluorescence Spectroscopy* (Springer US, Boston).
2. Boudker O, Ryan RM, Yernool D, Shimamoto K, Gouaux E (2007) Coupling substrate and ion binding to extracellular gate of a sodium-dependent aspartate transporter. *Nature* 445(7126):387–393.
3. Koch HP, et al. (1999) Differentiation of substrate and nonsubstrate inhibitors of the high-affinity, sodium-dependent glutamate transporters. *Mol Pharmacol* 56(6):1095–1104.
4. Vogt AD, Di Cera E (2012) Conformational selection or induced fit? A critical appraisal of the kinetic mechanism. *Biochemistry* 51(30):5894–5902.
5. Wanarska M, Hildebrandt P, Kur J (2007) A freeze-thaw method for disintegration of Escherichia coli cells producing T7 lysozyme used in pBAD expression systems. *Acta Biochim Pol* 54(3):671–672.
6. Reyes N, Oh S, Boudker O (2013) Binding thermodynamics of a glutamate transporter homolog. *Nat Struct Mol Biol* 20(5):634–640.
7. Pace CN, Vajdos F, Fee L, Grimsley G, Gray T (1995) How to measure and predict the molar absorption coefficient of a protein. *Protein Sci* 4(11):2411–2423.
8. Reyes N, Ginter C, Boudker O (2009) Transport mechanism of a bacterial homologue of glutamate transporters. *Nature* 462(7275):880–885.
9. Peterman BF (1979) Measurement of the dead time of a fluorescence stopped-flow instrument. *Anal Biochem* 93(2):442–444.
10. Fersht AR (1999) *Structure and Mechanism in Protein Science: A Guide to Enzyme Catalysis and Protein Folding* (Freeman, New York).
11. Compton ELR, Taylor EM, Mindell JA (2010) The 3-4 loop of an archaeal glutamate transporter homolog experiences ligand-induced structural changes and is essential for transport. *Proc Natl Acad Sci USA* 107(29):12840–12845.
12. Groeneveld M, Slotboom DJ (2010) Na^+:aspartate coupling stoichiometry in the glutamate transporter homologue Glt_{Ph}. *Biochemistry* 49(17):3511–3513.
13. Hoops S, et al. (2006) COPASI—a COmplex PAthway SImulator. *Bioinformatics* 22(24): 3067–3074.
14. Hindmarsh AC (1980) LSODE and LSODI, two new initial value ordinary differential equation solvers. *ACM SIGNUM Newsletter* 15(4):10–11.

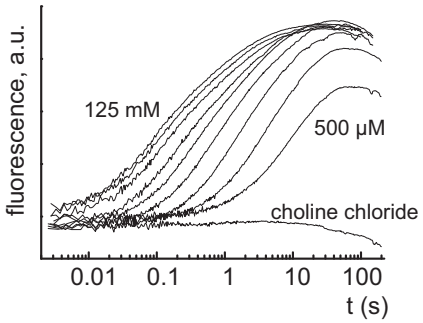

Fig. S1. $[Na^+]$ dependence of the slow processes preceding the amino acid binding to L130W Glt_{Ph}. Shown are the fluorescence traces after the simultaneous addition of 500 µM L-aspartate and various $[Na^+]$ to L130W Glt_{Ph}.

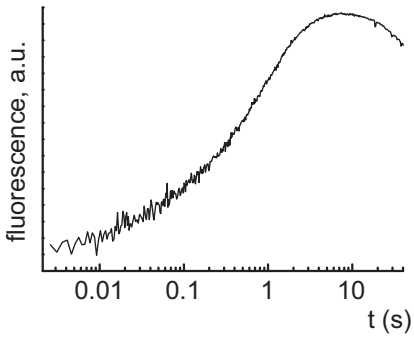

Fig. S2. Slow Na^+ binding to WT Glt_{Ph}. Representative fluorescence trace after the addition of 250 mM Na^+ to WT Glt_{Ph}. Excitation was 289 nm.

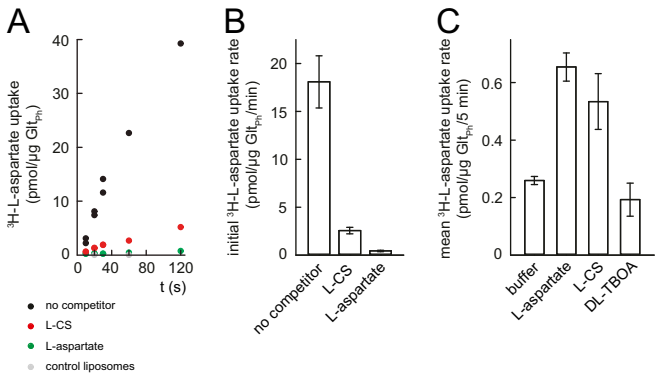

Fig. S3. L-CS specificity of Glt_{Ph}. (*A*) The time course of ^{3}H-L-aspartate (100 nM) uptake into GltPh-containing liposomes driven by an inwardly directed Na^+ gradient in the absence or presence of L-CS and L-aspartate (10 µM each). Shown are the first 120 s of a representative experiment with Glt_{Ph}-free liposomes as control. Duplicate measurements were performed for reaction times up to 30 s. (*B*) Initial rates of uptake in the absence or presence of competitor (mean ± SEM, three experiments). (*C*) Uptake of radiolabeled L-aspartate under counterflow conditions with buffer alone or buffer supplemented with L-aspartate, L-CS, or DL-TBOA (50 µM each) inside the proteoliposomes. Experiments were performed at equimolar Na^+ concentrations on both sides of the liposome. Data are given as mean ± SEM from six measurements after 5 min of reaction time in three experiments. The means of uptake with intraliposomal L-aspartate and L-CS are significantly different from the means of uptake with buffer or DL-TBOA inside the liposomes ($P < 0.05$ according to Tukey's Multiple Comparison Test, ANOVA one-way).

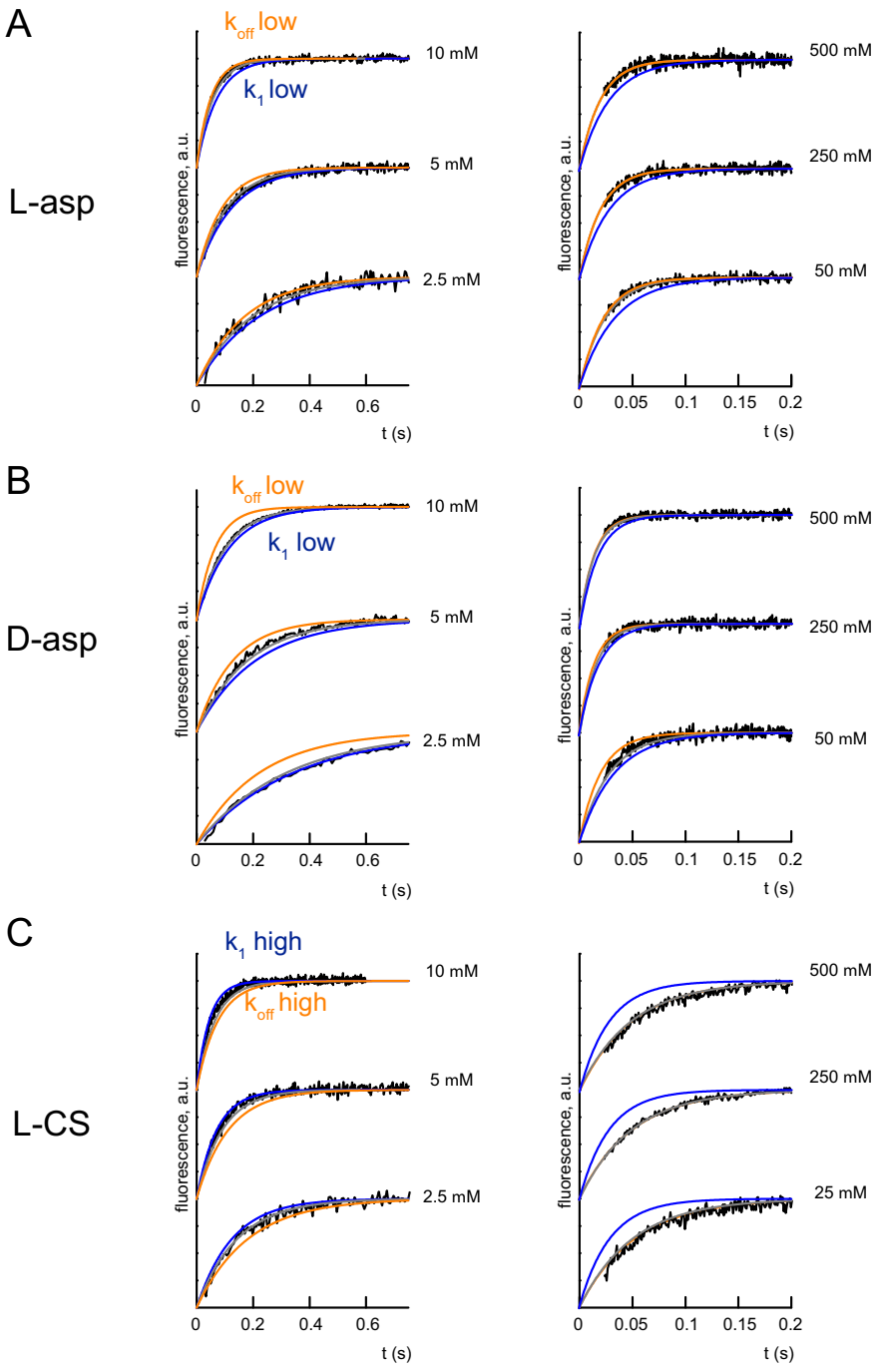

Fig. S4. The fluorescence changes predicted by Scheme **1** agree with experimental results. The results of the fluorescence simulations after addition of the indicated amino acids to Glt_{Ph} are shown together with the corresponding experimental traces (gray). The traces originating from the best fit parameters in Table 1 are in black, and the traces originating from varying k_{off} or k_1 are in orange or blue, respectively. The value of k_{off} was (*A* and *C*) 122 or (*B*) 417 s^{-1}. Values of k_1 were (*A* and *C*) 351 or (*B*) 623 s^{-1}.

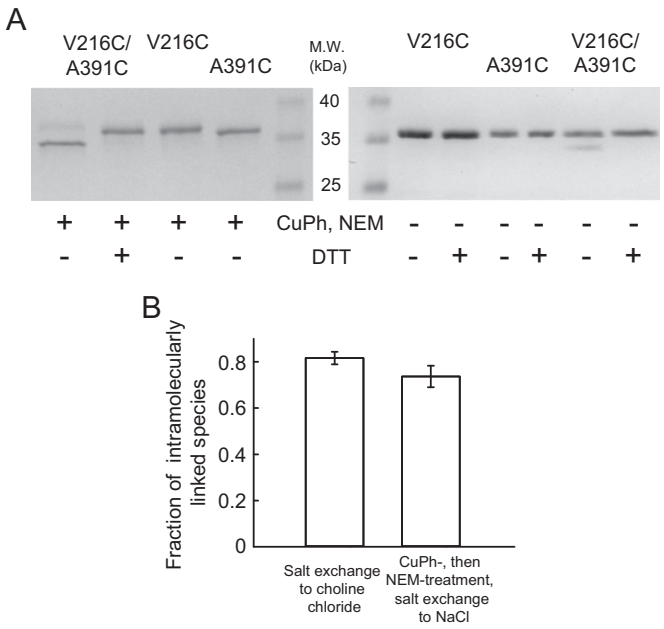

Fig. S5. An intramolecular disulfide bridge is formed by 75–80% of L130W V216C C321S A391C Glt_{Ph}. (*A*) Nonreducing SDS/PAGE showing double and single cysteine mutants (*Left*) after treatment aiming at cysteine oxidation or (*Right*) directly after elution from affinity resin. The SDS/PAGE sample buffer was with or without DTT as indicated. Note that the spontaneous formation of disulfide bridges in this mutant depends on the buffer conditions. (*Right*) In the presence of NaCl, the proportion of cross-linked species in the absence of DTT is lower than in the presence of ChCl (Fig. 4*E*). (*B*) Proportion of the cross-linked species as quantified by densitometry of Coomassie-stained gels like in *A Left*. Error bars represent SEM of two experiments.

Table S1. W130 fluorescence kinetics after the addition of 100 μM L-aspartate to protein preincubated with Na^+: best fit parameters of exponential fits to the data

[Na^+] (mM)	A*	$k^\dagger$	A	k	A	k	A	k	A	k	A	k	A‡	k
5														
Trial 1	0.290	0.043	0.259	0.172	0.178	0.662	0.246	2.628			0.028	77.760		
Trial 2	—	—	0.227	0.103	0.347	0.517	0.426	2.601	—	—	—	—		
Trial 3	0.108	0.028	—	—	0.319	0.301	0.227	1.579	0.233	6.365			0.114	523.560
Trial 4	—	—	0.188	0.137	0.515	0.720	0.182	1.986	—	—			0.116	333.026
Trial 5	—	—	0.205	0.114	0.318	0.476	0.358	2.144			0.014	62.854	0.105	384.615
10														
Trial 1	0.258	0.070	—	—	0.239	0.316	0.170	2.277	0.112	7.979			0.222	361.011
Trial 2	—	—	0.277	0.166	—	—	0.354	1.212	0.185	5.715			0.184	201.207
Trial 3	—	—	0.181	0.181	0.222	0.735	—		0.218	5.748			0.379	507.614
20														
Trial 1	0.214	0.083	—	—	0.233	0.505	—	—	0.163	6.144			0.389	265.252
Trial 2	—	—	—	—	0.356	0.353	—	—	0.389	4.835			0.255	107.875
Trial 3	—	—	—	—	0.227	0.411	—	—	0.147	4.194	0.045	53.792	0.580	534.759
40														
Trial 1	0.082	0.085			0.121	0.474	0.068	2.998			0.043	28.686	0.686	403.226
Trial 2					0.088	0.505			0.109	7.715			0.803	460.829
Trial 3					0.107	0.323	0.086	1.744	0.060	12.786			0.747	401.606
100														
Trial 1	0.019	0.093			0.045	0.628			0.025	4.508			0.911	400.000
Trial 2									0.107	5.921			0.893	448.430
Trial 3					0.058	0.978					0.024	21.834	0.919	450.450
200														
Trial 1					0.035	0.989					0.014	16.337	0.950	299.401
Trial 2													1.000	390.625
Trial 3					0.031	1.115							0.969	423.729
400														
Trial 1									0.014	5.109			0.986	364.964
Trial 2													1.000	456.621
Trial 3					0.006	1.057							0.994	396.825

*Amplitude.
†Rate constant.
‡Amplitude of largest rate was used in Fig. 2*C*.